The Journal of
Chemical Physics

Liquid–liquid criticality in the WAIL water model

Cite as: J. Chem. Phys. **157**, 024502 (2022); https://doi.org/10.1063/5.0099520
Submitted: 17 May 2022 • Accepted: 20 June 2022 • Accepted Manuscript Online: 20 June 2022 •
Published Online: 08 July 2022

Jack Weis, Francesco Sciortino, Athanassios Z. Panagiotopoulos, et al.

AIP Publishing

J. Chem. Phys. **157**, 024502 (2022); https://doi.org/10.1063/5.0099520 **157**, 024502

The Journal of Chemical Physics ARTICLE scitation.org/journal/jcp

Liquid–liquid criticality in the WAIL water model

Cite as: J. Chem. Phys. **157**, 024502 (2022); doi: 10.1063/5.0099520
Submitted: 17 May 2022 • Accepted: 20 June 2022 •
Published Online: 8 July 2022

Jack Weis,[1] Francesco Sciortino,[2] Athanassios Z. Panagiotopoulos,[1] and Pablo G. Debenedetti[1,a)]

AFFILIATIONS

[1] Department of Chemical and Biological Engineering, Princeton University, Princeton, New Jersey 08544, USA
[2] Department of Physics, Sapienza University of Rome, Piazzale Aldo Moro 2, I-00185 Roma, Italy

[a)]**Author to whom correspondence should be addressed:** pdebene@princeton.edu

ABSTRACT

The hypothesis that the anomalous behavior of liquid water is related to the existence of a second critical point in deeply supercooled states has long been the subject of intense debate. Recent, sophisticated experiments designed to observe the transformation between the two subcritical liquids on nano- and microsecond time scales, along with demanding numerical simulations based on classical (rigid) models parameterized to reproduce thermodynamic properties of water, have provided support to this hypothesis. A stronger numerical proof requires demonstrating that the critical point, which occurs at temperatures and pressures far from those at which the models were optimized, is robust with respect to model parameterization, specifically with respect to incorporating additional physical effects. Here, we show that a liquid–liquid critical point can be rigorously located also in the WAIL model of water [Pinnick *et al.*, J. Chem. Phys. **137**, 014510 (2012)], a model parameterized using *ab initio* calculations only. The model incorporates two features not present in many previously studied water models: It is both flexible and polarizable, properties which can significantly influence the phase behavior of water. The observation of the critical point in a model in which the water–water interaction is estimated using only quantum *ab initio* calculations provides strong support to the viewpoint according to which the existence of two distinct liquids is a robust feature in the free energy landscape of supercooled water.

I. INTRODUCTION

The possibility of multiple critical points in a one-component system is a fascinating topic permeating atomic,[1–4] molecular,[5,6] and colloidal science.[7–9] The presence of a second critical point in addition to the usual liquid–gas critical point indicates that distinct disordered liquid phases exist, differing in their properties at both the microscopic and macroscopic levels. Under suitable pressure (p) and temperature (T) conditions, the two liquids coexist. The fact that water, the most abundant liquid on the Earth's surface, might display such an unconventional behavior in deeply supercooled states[6] contributes to the relevance of this hypothesis.

The liquid–liquid transition (LLT) hypothesis explains water's anomalies as the effects of a liquid–liquid critical point (LLCP) found in the deeply supercooled liquid at elevated pressures. On cooling below the critical temperature at sufficiently high pressures, liquid water undergoes a first-order phase separation into low-density liquids (LDLs) and high-density liquids (HDLs), both still metastable with respect to crystalline ice. A liquid–liquid critical point indeed influences a large region of the phase diagram,[10] inducing a critical p and T dependence in several response functions (compressibility, specific heat, thermal expansivity) and explaining in an elegant framework the well-known thermodynamic anomalies of water.[11–13] Similarly, the existence of distinct liquid states suggests the existence of corresponding, structurally distinct water glasses, consistent with the observed phenomenon of polyamorphism.[14–16] Recent sophisticated pump-and-probe experiments[17] have provided strong evidence that a suitably prepared high-density disordered liquid water, under deeply supercooled conditions, transforms into a structurally distinct and less dense liquid state before freezing into ice.

Numerical studies have played an important role in the development of the idea that a single-component system can organize itself into more than one disordered phase, particularly when those phases are metastable liquids. Compared to experiments, numerical studies are based on truly clean samples and, due to the use of periodic boundary conditions, can easily be conducted without confining interfaces and as such are not affected by heterogeneous nucleation. In addition, they provide access to the short time scales in which the liquid has sufficient time to equilibrate in a metastable sense, but not for homogeneous nucleation of the stable phase to occur.

Despite these positive aspects, numerical studies have a few major drawbacks. The sluggish dynamics associated with critical points require extensive computational resources and, more importantly, the approximations of reality inherent in the choice of the water–water interaction potential unavoidably make simulations an approximate tool for studying real systems of interest. It is, thus, important to verify whether the recent results[18] demonstrating the existence of critical fluctuations in classical rigid water models designed to reproduce selected experimental results[19,20] stand up when the model does not result from a fit to selected experimental data but is instead designed by incorporating *ab initio* quantum mechanical calculations of water's potential energy surface.

A preliminary step in this direction has been recently provided by combining density functional theory (DFT), machine learning, and molecular simulations, exploiting the power of a deep neural network model to represent the DFT *ab initio* potential energy surface of water.[21] This state-of-the-art study reported strong evidence of the existence of two distinct liquid states but could not provide a rigorous proof of the liquid–liquid critical point due to the heavy numerical load required to explore low-temperature states.

With the aim of demonstrating the existence of a liquid–liquid critical point using models that are not fitted to experimental data but rather obtained from the underlying electronic structure potential energy surface, we investigate here the WAIL model.[22] WAIL is a flexible, four-site model with a negatively charged site located between two OH bonds and positive charges on the hydrogen sites.[22,23] The location of the negative site is a linear combination of the OH vectors. Bond flexibility is modeled via a fourth-order stretching expansion and a harmonic H–O–H term. Intermolecular interactions are modeled via a combination of Buckingham O–O term, point charge Coulombic contributions, and a repulsive term between hydrogen atoms in one molecule and the negatively charged site on another molecule. Model parameters were obtained via the adaptive force matching method[22] by fitting to post-Hartree–Fock quality forces obtained from quantum mechanics/molecular mechanics (QM/MM) calculations rather than empirically reproducing selected thermophysical properties. WAIL also predicts radial distribution functions (RDFs) and heats of vaporization for both ice and liquid in good agreement with experiments. Unlike previously investigated classical models based on rigid molecules, the WAIL model incorporates polarizability via a negatively charged site and allows for stretching and bending of the hydrogen bonds, a significant increase in the complexity of the modeling of the water–water interaction potential.[22,23]

Evidence consistent with a liquid–liquid transition in a region of temperature and pressure currently accessible to extensive numerical studies has been reported for this model,[24] making it a good candidate for rigorously demonstrating, for the first time, critical behavior in a model parameterized only on *ab initio* calculations.[25] In this work, we demonstrate the presence of a LLCP in the first-principles WAIL model and rigorously locate it, strengthening the description of water's anomalies as radiating out from a critical point in the deeply supercooled liquid, below which two distinct liquid forms exist.

II. METHODS

Long correlation times are a defining feature of systems near critical points, and low temperatures cause sluggish dynamics. Simulations near the critical point are, therefore, computationally expensive. To minimize the number of long exploratory simulations in the relative vicinity of the critical point, a two-state equation of state[10,26,27] (TSEOS) approach was first used to provide an estimate of the location of the liquid–liquid critical point of the WAIL model. This estimate allowed for more rigorous, but more computationally intensive, investigations of criticality carried out in a more targeted manner.

A. Two-state equation of state

The TSEOS[10,26,27] models a substance as a mixture of two distinct but interconvertible components A and B and expresses the Gibbs free energy G of the system as the following function of temperature, pressure, and the fraction of molecules in the B local configuration x:

$$G = G^{A} + xG^{BA} + G^{mix}, \tag{1}$$

$$G^{A} = RT_c \sum_{j,k} c_{jk} \left(\Delta\hat{T}\right)^{j} \left(\Delta\hat{p}\right)^{k}, \tag{2}$$

$$G^{BA} = RT\lambda\left(\Delta\hat{T} + a\Delta\hat{p} + b\left(\Delta\hat{T}\right)\left(\Delta\hat{p}\right)\right), \tag{3}$$

$$G^{mix} = RT\left(x\ \ln\ x + (1-x)\ln(1-x) + \frac{2+\omega_0\Delta\hat{p}}{T/T_c}x(1-x)\right). \tag{4}$$

Here, G^{A} represents the Gibbs free energy of structure A, G^{BA} is the Gibbs free energy difference between structures B and A, and G^{mix} is the free energy change due to mixing. The fit parameters are a, b, λ, ω_0, and c_{jk}, where j and k go from 0 to 4. The reduced pressure $\Delta\hat{p}$ is defined as $\frac{p-p_c}{p_c}$ and the reduced temperature $\Delta\hat{T}$ as $\frac{T-T_c}{T_c}$. Further details on the fitting procedure can be found in Appendix A. The TSEOS was fitted to the observed density and energy per particle and predicted a critical point at $p_c = 356$ bar and $T_c = 208.5$ K. The results of the fit are shown in Fig. 1; the best fit parameters are given in Table III.

The thermodynamic properties of the system can be calculated from the TSEOS as derivatives of G; see Appendix A for details. Only positive pressures were considered in fitting the TSEOS to minimize the influence of the liquid–vapor spinodal, which could be accounted for explicitly in more advanced versions of the TSEOS.[26] The good fit obtained without consideration of the liquid–vapor spinodal suggests that it would not have played an important role in the positive-pressure–low-temperature region of interest in this work.

The two-state model assumes the existence of a critical point; the changing fraction of molecules in the B local environment, here identified with low-density configurations, is the main driver of changing physical properties upon approaching the critical point.[27,28] The low-density fraction (x) is calculated explicitly in the TSEOS, as shown in Fig. 1. The correspondence between high x at low temperatures and pressures and the falling density of the liquid

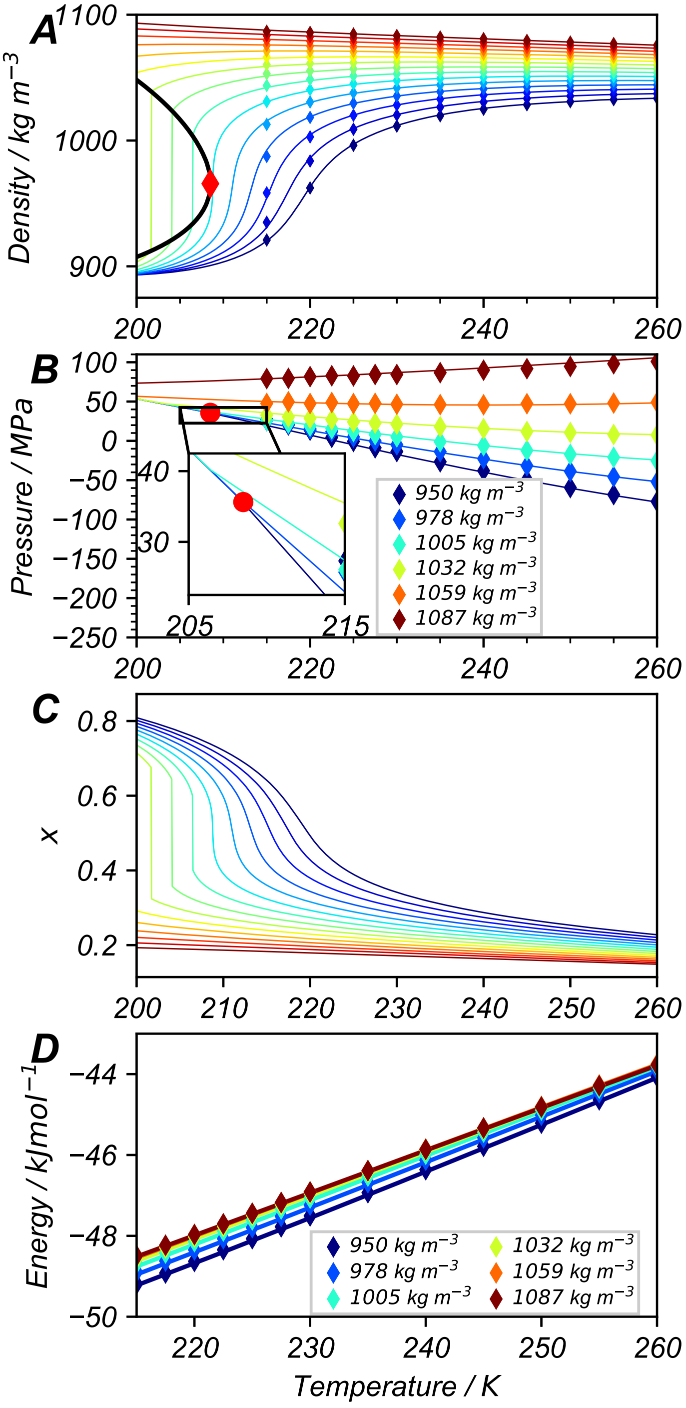

FIG. 1. TSEOS fit to simulation data, rescaled to H_2O. (a) Density along isobars from MTMB data and (b) along isochores. Isobars in (a) range from 100 (blue) to 800 bar (red) with a spacing of 50 bar; crossing of isochores [inset, (b)] is a signature of criticality. (c) Equilibrium fraction of molecules with a low-density local environment, as predicted by the TSEOS model, with isochores from 100 to 800 bar as in (a). At low temperatures and pressures, the TSEOS predicts that WAIL shifts to a liquid composed primarily of low-density structures, producing a density maximum and related anomalies. (d) Energy (kinetic + potential) along isochores.

upon cooling is apparent. This equation of state captures many of the thermodynamic anomalies associated with water, for example, progressively sharper compressibility extrema on pressurization, as shown in Fig. 4 in Appendix A.

B. MD simulations for the TSEOS

The TSEOS was fit to density and energy data along isochores and isobars, as shown in Fig. 1. Initial configurations were generated by steepest-descent energy minimization followed by an equilibration period of 100 ns; the simulation box contained 256 molecules. Isobar data spaced every 50 bar and 5 K were generated for use in the TSEOS fitting procedure using the on-the-fly probability enhanced sampling (OPES) technique[29] applied in the multithermal–multibaric (MTMB) ensemble within the variationally enhanced sampling module in PLUMED.[30–32] Additional details on this procedure are provided in Appendix B. Pressures sampled in the OPES simulation ranged from −200 to 800 bars and temperatures from 215 to 350 K; note that the pressure range explored with OPES was greater than that used to parameterize the TSEOS. On-the-fly probability enhanced sampling (OPES) provides a more computationally efficient way to sample a large region of phase space by introducing a biasing potential $B(U, V)$ to ensure that the system fully explores the relevant energies and densities.[29] The biasing potential is dynamically updated as the system explores the phase space; estimates of observables generated in this way are valid once the biasing potential (and hence their values) converges. This simulation was run for 475 ns—an order of magnitude longer than was required for the biasing potential to converge but much shorter than was required for direct observation of low- and high-density states near the critical point.

Isochore data were generated using replica-exchange molecular dynamics with an exchange move attempted every 500 steps.[33] Water was modeled as D_2O by increasing the weight of the hydrogen atoms by 1.0 AMU; the potential was not otherwise modified to consider nuclear quantum effects.[22] The heavier deuterium atoms served purely to allow for a longer simulation time step. All results, however, have been appropriately rescaled to reflect the molecular weight of H_2O and are presented in this rescaled form throughout this work.

C. Rigorous critical point estimation

Critical points in fluids with short-range interactions and described by a scalar order parameter are known to belong to the 3D Ising universality class.[34] Because of the absence of hole–particle symmetry, the relevant order parameter for fluids is a linear combination of density and energy $M = \frac{\rho}{\rho_0} + s\frac{E}{E_0}$, where E is the energy per molecule, s is the so-called field-mixing parameter and ρ_0 and E_0 are characteristic density and energy scales, making M dimensionless.[35] One then seeks, numerically, for the combination of temperature T_c, pressure p_c, and s that best fits the universal Ising distribution of the magnetization at the critical point,[36] using a rescaled M with zero mean and unit variance as the fluid order parameter.[35] The statistics of energy and density fluctuations at different thermodynamic conditions (T, p) are obtained from numerical data using the histogram reweighting method.[37] The details of the histogram reweighting procedure are described below and in

Appendix C and the procedure for locating the critical point from the reweighted data is provided in Appendix D.

Simulations close to the critical point were equilibrated for one microsecond and run for 2–12 μs using standard molecular dynamics in the NPT ensemble. Joint histograms of total energy and density were then generated and used to estimate the density of states in this region using the weighted histogram analysis method.[37–39] Further details on this technique are provided in Appendix C. The approximation of the density of states obtained from multiple-histogram analysis was then reweighted to predict the observed energy and density at nearby conditions, including the critical point itself. The critical point was identified by varying the reweighted temperature and pressure and the field-mixing parameter s to best reproduce the critical Ising distribution.[36] This process was repeated for three distinct system sizes ($N = 300, 512, 1000$ molecules) to assess any finite-size effect on the location of the critical point; such effects have been known to arise from the interaction of diverging length scales associated with criticality and the short length scales imposed by the simulation box size.[40] Details of the simulation trajectories used are given in Appendix E and the fitting procedure is described in Appendix D.

D. Details of the molecular dynamics simulations

All simulations aimed at collecting near-critical density and energy histograms were performed with Gromacs 5.1.4.[41–46] Water was modeled as D_2O using the WAIL potential with a time step of 1 fs and a cutoff of 1 nm for van der Waals interactions and short-range Coulomb electrostatic interactions.[22,24] Long-range electrostatics were incorporated using the Particle-Mesh Ewald (PME) method with a cutoff distance of 0.9 nm and fourth-order interpolation. Temperature coupling was performed using the Nosé–Hoover thermostat[47,48] with $\tau_T = 8.011$ ps. Pressure coupling was incorporated with the Parrinello–Rahman barostat[49] using $\tau_p = 18.3$ ps and a compressibility of 4.5×10^{-5} bar^{-1}, as have previously been used to examine the LLCP in water using Gromacs.[18] Here, as there, non-integer time constants were chosen to minimize the possibility of resonance between the time scale of the barostat and that of the thermostat. All simulations used periodic boundary conditions.

III. RESULTS AND DISCUSSION

Before proceeding with a rigorous analysis of the critical fluctuations, the TSEOS was fit to thermodynamic data of the WAIL model at relevant temperatures and pressures.[50] In this approach, the Gibbs free energy is written as the mole fraction-weighted sum of the free energy of the molecules in the two different local environments—the low-density–low-energy environment (B) and in the high-density–high-energy one (A) previously discussed—weighted, respectively, with composition x and $1 - x$ and supplemented by a mean-field mixing contribution G^{mix}, which incorporates a non-ideality term, as described in the Sec. II.

Figure 1 compares the equation of state in the $\rho - T$ (a) and $p - T$ (b) planes resulting from MD simulations with the best fit based on the two-state mean-field free energy expression in Eqs. (1)–(4), previously used to model TIP4P/2005.[27] Figure 1(d) provides an analogous comparison for the energy. The quality of the fit is remarkable and the estimated critical temperature and pressure are in good agreement with the results obtained by comparison to the critical Ising distribution, calculated as described in Appendix D. The TSEOS results vividly demonstrate how water's anomalous properties, such as the compressibility maxima and the density maxima along isobars, ultimately radiate out from the LLCP.[51]

Close to a critical point, the structure of the system is characterized by long-wavelength fluctuations.[52] In fluids, at fixed T and p, this results in spatial fluctuations in both energy and density. Following a well-established procedure,[35] we estimate the fluctuations

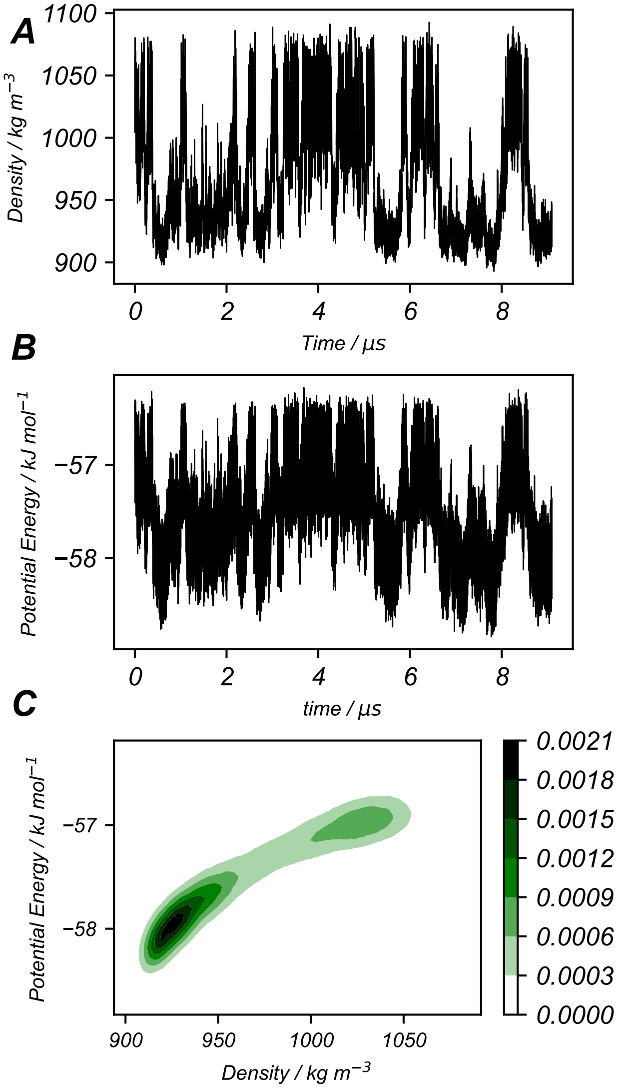

FIG. 2. Fluctuations at 380 bar and 210 K, rescaled to H_2O, near the critical point for a system with $N = 1000$. Density (a) and potential energy (b) fluctuations show bimodality and long correlation times. (c) Joint energy–density histogram calculated from the same trajectory highlighting the bimodality and the positive correlation between density and potential energy.

of an appropriately normalized order parameter (a linear combination of density ρ and potential energy per particle E) searching for p and T values where the known bimodal distribution typical of the Ising universality class at a critical point is observed.[35] An example of the evolution in time of the density and the energy is shown in Fig. 2, together with the distribution probability in the E, ρ plane for T = 210 K and p = 380 bar.

Both quantities fluctuate in a correlated way, showing clear bimodality, with a correlation time of the order of microseconds. On this time scale, the system flips between low- and high-density and low- and high energy states. This bimodality, once again, is indicative of an approaching phase transition and an associated first-order coexistence curve between two liquids: one characterized by low energy and low density and the other characterized by high energy and high density.[11,12] We note that an order parameter of the form $t \equiv \rho + sE$ (where s is the so-called field-mixing parameter) rather than ρ or E alone is needed to recover Ising-like behavior, as discussed in the Sec. II.[35]

As described in detail in Appendix C, we calculate the density of states $\Omega(E, \rho)$ by combining several energy–density histograms at conditions expected to be near the critical point using the weighted histogram analysis method.[37,38] The fluctuations observed in several μs-long runs differing in T and p are, thus, expected to be representative of the structures of importance to the critical point.[18,53,54] The density of states is then used to predict the observed distributions of energy and density at arbitrary (T, p), provided they are sufficiently close to the sampled range.

This predicted energy–density histogram is then used to generate a histogram of the order parameter t and compared with the universal distribution of the fluctuations characteristic of the Ising universality class, resulting in a best fit estimate of the critical temperature T_c, critical pressure p_c, and critical density ρ_c. The results of these fits for the three different system sizes considered here are presented in Fig. 3 and in Table I; this fitting procedure also produces an estimate for the field-mixing parameter s. An accurate numerical representation of the 3D critical Ising distribution[36] was obtained for system sizes of N = 300, 512, and 1000 molecules, with the conditions producing the best fit to the Ising curve taken to be the location of the critical point.

TABLE I. Best fit critical point parameters for the WAIL model.

System	T_c (K)	p_c (bar)	ρ_c (kg m^{-3})	s
N = 300	210.2 ± 3	357 ± 26	1001 ± 45	94 ± 78
N = 512	210.6 ± 2	369 ± 21	981 ± 50	83 ± 66
N = 1000	210.7 ± 2	368 ± 18	1006 ± 37	79 ± 43

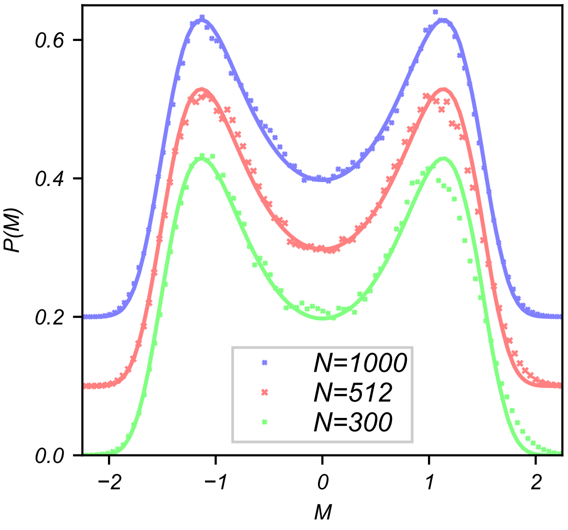

FIG. 3. Optimization of (p_c, T_c, s) produces a good fit to the Ising curve for each system size examined. N = 512 is shifted up by 0.1; N = 1000 is shifted up by 0.2. The order parameter M is the linear combination of density and energy $\frac{\rho}{\rho_0} + s\frac{E}{E_0}$ rescaled to unit variance and zero mean. Here, ρ_0 = 1 kg m^{-3} and E_0 = 1 kJ mol^{-1}. Lines represent the universal 3D Ising distribution;[36] points are reweighted simulation data.

Notably, the observed critical temperatures are all within 0.3 K of 210.5 K and within 8 bar of 365 bar. In light of this weak system-size dependence, no attempt is made at explicitly determining the dependence of T_c and p_c on the system size. Interestingly, the WAIL model predicts a LLCP at a much lower pressure than all previously studied water models and in closer agreement with estimates based on experimental data[55] and with the theoretical work of Holten *et al.*[56] This critical temperature and pressure are also located near the 205 K, 500 bar estimate previously published for WAIL on the basis of enhanced fluctuations in this region.[24]

Identification of the critical point in this manner provides unambiguous proof that the WAIL model, with flexible bonds reminiscent of those in real water, shows an LLCP. Previously, this had only been proven in classical water models with rigid bonds. Evidence suggesting an LLT in WAIL had previously been obtained, but the critical point had not been rigorously located.[24] Table II lists the liquid–liquid critical temperature and pressure for a number of water models. Of these, only TIP4P/2005, TIP4P/Ice, and WAIL have rigorously located critical points; the locations of the critical points in the other models have been estimated using phenomenological models such as the two-state equation of state only.

TABLE II. Critical parameters obtained in previous water model studies.[a]

Model	T_c (K)	p_c (bar)
TIP4P/2005[18]	172	1861
TIP4P/Ice[18]	188.6	1725
E3B3[57]	180	2100
iAMOEBA[58]	184	1750
DeePMD[21]	224	2687
ST2[59]	237	1670
WAIL[b]	210.5	365

[a] Italics denote approximate calculations (e.g., TSEOS fits).
[b] This work.

IV. CONCLUSION

In summary, we have robustly demonstrated that the free energy of the WAIL model—a model which incorporates flexibility and polarizability and is based only on quantum mechanical calculations—is characterized by two liquid phases separated by a first-order line ending in a critical point at $p_c = 365$ bar and $T_c = 210.5$ K. Thus, the validity of the thermodynamic scenario originally proposed to describe the behavior of supercooled water on the basis of a numerical study of the historical ST2 model[6] and recently confirmed in a study of two realistic classical rigid water models TIP4P/2005 and TIP4P/Ice[18] is significantly reinforced by the present results. Finally, we emphasize that all other previously investigated models for which the critical point has been unambiguously determined locate the critical point at significantly higher pressure (about 1800 bar or above)[6,18] than the current WAIL predictions. Such a difference in critical pressure not only highlights the important role played by molecular flexibility and polarizability but also brings numerical predictions closer to the most recent experimentally based estimates.[60–62]

Further work should consider the use of models incorporating other important behaviors found in real water, in particular, nuclear quantum effects. Examination of the crystallization of ice in this region—as the main reason for the lack of experimental data on real water—also merits further investigation.

ACKNOWLEDGMENTS

F.S. acknowledges support from Ministero Istruzione Università Ricerca—Progetti di Rilevante Interesse Nazionale (Grant No. 2017Z55KCW) and acknowledges IscrB-CINECA for providing numerical resources. J.W. and P.G.D. acknowledge support from the U.S. National Science Foundation Award No. CHE-1856704. Their calculations were performed on computational resources managed and supported by Princeton Research Computing, a consortium of groups including the Princeton Institute for Computational Science and Engineering (PICSciE) and the Office of Information Technology's High Performance Computing Center and Visualization Laboratory at Princeton University.

AUTHOR DECLARATIONS

Conflict of Interest

The authors have no conflicts to disclose.

Author Contributions

Jack Weis: Conceptualization (equal); Data curation (lead); Formal analysis (equal); Investigation (lead); Methodology (equal); Project administration (supporting); Software (equal); Validation (equal); Visualization (equal); Writing – original draft (lead); Writing – review & editing (equal). **Francesco Sciortino:** Conceptualization (supporting); Data curation (supporting); Formal analysis (equal); Funding acquisition (supporting); Investigation (supporting); Methodology (equal); Project administration (supporting); Resources (supporting); Software (equal); Supervision (supporting); Validation (supporting); Writing – original draft (supporting); Writing – review & editing (equal). **Athanassios Z. Panagiotopoulos:** Conceptualization (supporting); Formal analysis (supporting); Investigation (supporting); Methodology (equal); Supervision (equal); Validation (supporting); Writing – review & editing (equal). **Pablo G. Debenedetti:** Conceptualization (equal); Funding acquisition (lead); Methodology (equal); Project administration (equal); Resources (lead); Supervision (equal); Writing – review & editing (equal).

DATA AVAILABILITY

The data that support the findings of this study are openly available at https://doi.org/10.34770/vsj7-4j83.

APPENDIX A: TSEOS FIT RESULTS

The two-state model was fit to the total energy per particle and density of the system at given pressure and temperature, as shown in the main text. These quantities were calculated numerically as derivatives of the Gibbs free energy predicted by the equation of state as follows:

$$V = \left(\frac{\partial G}{\partial p}\right)_T, \tag{A1}$$

$$E = G - T\left(\frac{\partial G}{\partial T}\right)_p - p\left(\frac{\partial G}{\partial p}\right)_T. \tag{A2}$$

The coefficients of the TSEOS were optimized using the Nelder–Mead algorithm in Scipy,[63] and the final results are provided in Table III.

The expected thermodynamic anomalies of water, such as a density maximum and sharp divergence of the response functions,

TABLE III. Optimized TSEOS parameters.

Parameter	Value
T_c (K)	208.5
p_c (bar)	356.3
λ	1.795
a	7.88×10^{-2}
b	-6.94×10^{-2}
ω_0	5.10×10^{-2}
c_{00}	-27.9
c_{01}	3.00×10^{-1}
c_{02}	2.20×10^{-3}
c_{11}	7.54×10^{-2}
c_{20}	-6.62
c_{12}	1.22×10^{-2}
c_{21}	2.01×10^{-2}
c_{30}	2.10
c_{22}	1.03×10^{-2}
c_{31}	1.17×10^{-2}
c_{40}	-49.5×10^{-1}
c_{23}	7.54×10^{-2}
c_{32}	9.82×10^{-4}
c_{33}	-8.92×10^{-4}

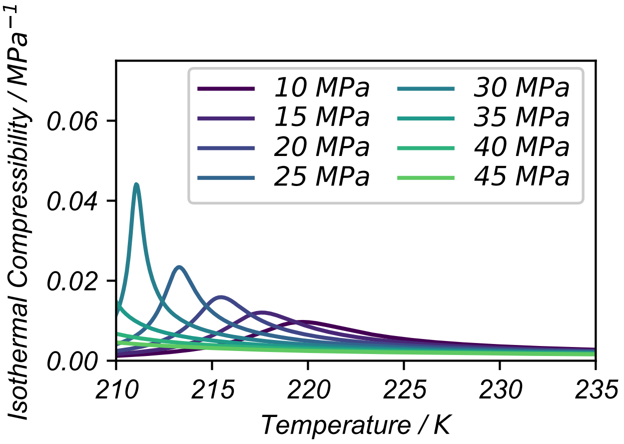

FIG. 4. Temperature dependence of the compressibility along isobars, as predicted by the TSEOS.

are clearly visible in the TSEOS predictions. Sharp increases in the isothermal compressibility, for example, can be seen in Fig. 4.

APPENDIX B: MULTITHERMAL–MULTIBARIC SAMPLING

The multithermal–multibaric ensemble was implemented as the TD_MULTITHERMAL_MULTIBARIC distribution in the variationally-enhanced sampling (VES) module within Plumed.[30–32] Gromacs was patched with Plumed version 2.6[31,32] and a simulation of 256 molecules was run for 475 ns on a temperature range from 215 to 350 K and a pressure range from −200 to 800 bar, with a nominal temperature of 300 K and a nominal pressure of 200 bar.[21] The energy–volume space thus sampled is shown in Fig. 5. Note that only positive pressures were used to parameterize the TSEOS; the inclusion of a wider range of pressures in the MTMB calculations was done to ensure good sampling at all pressures considered in the TSEOS.

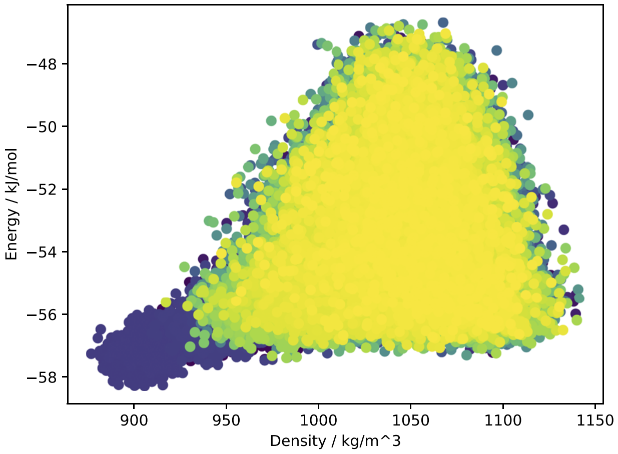

FIG. 5. Conditions sampled by OPES in the multithermal–multibaric ensemble, with the most recent shown in yellow. Note that virtually the entire state space used was sampled by the end of the simulation. Densities rescaled to H_2O.

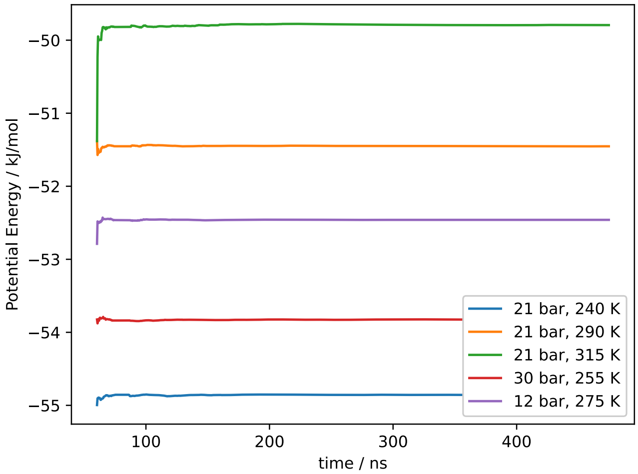

FIG. 6. Potential energies at selected (T, p) conditions, computed over a given trajectory length. Note that all predictions have converged by 100 ns.

The Q6 order parameter was used to detect ice; a potential wall was used to prevent the system from sampling configurations with average Q6[64] greater than 0.125 to avoid ice. This potential wall was implemented with the Plumed UPPER_WALLS command[32] with $k_i = 20\,000$ and $a_i = 0.125$.[21] Convergence of the simulation was determined by monitoring the convergence of the calculated potential energy at several points throughout the (p, T) regime of interest, as shown in Fig. 6.

The multithermal–multibaric scheme calculates the value of an observable O at a reweighted temperature and pressure (T', p') by weighted averaging observed values at the nominal conditions (T, p) and weights w for each observed configuration $\mathbf{R}$,

$$\langle O(\mathbf{R}, V)\rangle_{T',p'} = \frac{\langle O(\mathbf{R}, V)w(\mathbf{R}; V)\rangle_{T,P}}{\langle w(\mathbf{R}, V)\rangle_{T,P}}. \tag{B1}$$

The weighting function is calculated from a biasing potential $B(U, V)$ biasing the potential energy and volume of the system.[30] It is generated dynamically by OPES.[29]

The weight function w, where $\beta = 1/k_B T$, was calculated from the bias potential as

$$w(\mathbf{R}) = e^{(\beta-\beta')U(\mathbf{R})+(\beta p-\beta' p')V(\mathbf{R})} e^{\beta B(U(\mathbf{R}),V)}. \tag{B2}$$

APPENDIX C: HISTOGRAM REWEIGHTING

Histogram reweighting uses the partition function of the system to predict its behavior at arbitrary conditions provided from its behavior under one set of conditions. In the NPT ensemble, the relevant partition function is

$$Z(p,\beta) = \sum_V \sum_E \Omega(V,E) e^{-\beta(E+pV)}. \tag{C1}$$

Here, the partition function $Z(p,\beta)$ is defined in terms of the density of states $\Omega(V,E)$, where $\beta = 1/k_B T$ and T is the system temperature, p its pressure, V its volume, and E its potential energy. This corresponds to the following probability distribution function $P(V,E)$ of energy and volume at a given pressure and temperature:

$$P(V,E;p,\beta) = \frac{\Omega(V,E)e^{-\beta(E+pV)}}{Z(p,\beta)}. \tag{C2}$$

For a given simulation trajectory i, an approximation of the partition function can be constructed as follows:

$$Z(p_i,\beta_i) = \sum_V \sum_E \Omega(V,E) e^{-\beta_i(E+p_iV)} = e^{-\beta_i G(p_i,\beta_i)}. \tag{C3}$$

In the NPT simulations used here, pressure and temperature are held constant and energies and densities can be calculated for a given configuration. The density of states $\Omega(E,V)$ requires additional information on the frequency at which configurations corresponding to a given energy and density appear in the simulation trajectory. By approximating $P(V,E;\ p,\beta)$ as the normalized histogram of the observed energy and volume fluctuations $\frac{H(E,V;p,\beta)}{N_{obs}}$ at temperature T and pressure p, the density of states can be calculated. Here, the histogram value $H(E,V;\ p,\beta)$ is defined as the number of configurations observed with densities and energies falling into the histogram bin containing energy E and volume V; 200 histogram bins each in density and energy were used here. This histogram is normalized by the total number of configurations N_{obs} considered. Here, configurations were taken every 40 ps in the trajectory after an equilibration period of 400 ns. For a given trajectory i, this becomes

$$\Omega_i(E,V) = \frac{H_i(E,V)}{N_i} e^{\beta_i(E+p_iV)} e^{-\beta_i G(p_i,\beta_i)}. \tag{C4}$$

To arrive at a single consensus for the density of states $\Omega(E,V)$ for the system, each run is assigned a weight factor $\omega_i \geq 0$ such that $\sum_i \omega_i = 1$. $\Omega(E,V)$ can then be expressed as the following linear combination of the weighted histograms:

$$\Omega(E,V) = \sum_i \omega_i \Omega_i(E,V) = \sum_i \omega_i \frac{H_i(E,V)}{N_i} e^{\beta_i(E+p_iV)} e^{-\beta_i G(p_i,\beta_i)}. \tag{C5}$$

Minimizing the variance of $\Omega(E,V)$ produces coupled equations that must be solved self-consistently, enabling an optimal $\Omega(E,V)$ to be identified, allowing $P(V,E;\ p,\beta)$ to be calculated at arbitrary conditions. This is identically the joint density–energy distribution that is needed for identification of a critical point,[37–39]

$$\begin{cases} \Omega(E,V) = \dfrac{\sum_i H_i(E,V)}{\sum_i N_i e^{\beta_i(E+p_iV)} e^{-\beta_i G(p_i,\beta_i)}}, \\ e^{-\beta_i G(p_i,\beta_i)} = \sum_V \sum_E \Omega(E,V) e^{-\beta_i(E+p_iV)}. \end{cases} \tag{C6}$$

TABLE IV. Trajectory specifications, $N = 300$.

Pressure (bar)	Temperature (K)	Length (μs)
1	220	3.0
100	205	2.1
100	210	2.9
100	220	1.1
200	205	2.1
200	210	2.4
300	220	1.4
400	205	2.3
400	210	2.1
500	205	1.1
500	210	0.7
500	220	0.5
600	205	1.4

APPENDIX D: ISING CURVE FITTING

The probability density of the magnetization of a critical Ising ferromagnet is a characteristic of any critical point belonging to the Ising universality class, including liquid–liquid and liquid–gas critical points.[34] The 3D Ising curve at the critical point can be accurately approximated as the following continuous function:[36]

$$P(M) = Ae^{-\left(\frac{M^2}{M_0^2}-1\right)^2 \left(a\frac{M^2}{M_0^2}-c\right)^2}, \tag{D1}$$

where $a = 0.158$, $c = 0.776$, $M_0 = 1.134\,165\,5$, and the normalization constant $A = 1132.487$. Here, the value of the constant M_0 was chosen to give the distribution unit variance.

For a fluid critical point such as an LLCP, a suitable order parameter is a linear combination of density and (per particle) energy: $t = \rho + sE$, where s is not known *a priori*. Choosing an arbitrary

TABLE V. Trajectory specifications, $N = 512$.

Pressure (bar)	Temperature (K)	Length (μs)
300	205	2.0
350	205	2.1
400	205	2.1
450	205	2.0
300	210	10.1
350	210	11.5
375	210	5.0
400	210	11.3
450	210	9.8
150	215	2.8
200	215	2.8
250	215	2.3
300	215	4.7
350	215	4.7

TABLE VI. Trajectory specifications, $N = 1000$.

Pressure (bar)	Temperature (K)	Length (μs)
150	215	1.2
200	215	1.2
335	210	5.2
335	215	2.7
335	220	2.4
350	210	5.2
350	215	2.7
350	220	2.3
365	210	7.6
365	215	2.7
365	220	1.7
380	210	5.6
380	215	2.7
380	220	1.6
395	210	4.5
395	215	1.9
410	210	3.0

initial value of s, the scale of M is chosen so that it has zero mean and unit variance,

$$M = \frac{t - \langle t \rangle}{\sigma_t}. \tag{D2}$$

Here, $\langle t \rangle$ represents the arithmetic mean and σ_t the standard deviation of $t = \rho + sE$. The values of T, p, and s were optimized using the MINUIT optimization code.[65]

APPENDIX E: TRAJECTORIES USED

Molecular dynamics trajectories at the following conditions were used to rigorously locate the critical point. Simulations with 300 molecules are described in Table IV, simulations with 512 molecules in Table V, and those with 1000 molecules in Table VI.

REFERENCES

[1] Y. Katayama, T. Mizutani, W. Utsumi, O. Shimomura, M. Yamakata, and K.-i. Funakoshi, "A first-order liquid–liquid phase transition in phosphorus," Nature **403**, 170–173 (2000).

[2] L. Henry, M. Mezouar, G. Garbarino, D. Sifré, G. Weck, and F. Datchi, "Liquid–liquid transition and critical point in sulfur," Nature **584**, 382–386 (2020).

[3] C. J. Wu, J. N. Glosli, G. Galli, and F. H. Ree, "Liquid-liquid phase transition in elemental carbon: A first-principles investigation," Phys. Rev. Lett. **89**, 135701 (2002).

[4] M. Beye, F. Sorgenfrei, W. F. Schlotter, W. Wurth, and A. Föhlisch, "The liquid-liquid phase transition in silicon revealed by snapshots of valence electrons," Proc. Natl. Acad. Sci. U. S. A. **107**, 16772–16776 (2010).

[5] J. Russo, K. Akahane, and H. Tanaka, "Water-like anomalies as a function of tetrahedrality," Proc. Natl. Acad. Sci. U. S. A. **115**, E3333–E3341 (2018).

[6] P. H. Poole, F. Sciortino, U. Essmann, and H. E. Stanley, "Phase behaviour of metastable water," Nature **360**, 324–328 (1992).

[7] C. W. Hsu, J. Largo, F. Sciortino, and F. W. Starr, "Hierarchies of networked phases induced by multiple liquid-liquid critical points," Proc. Natl. Acad. Sci. U. S. A. **105**, 13711–13715 (2008).

[8] F. Smallenburg, L. Filion, and F. Sciortino, "Erasing no-man's land by thermodynamically stabilizing the liquid–liquid transition in tetrahedral particles," Nat. Phys. **10**, 653–657 (2014).

[9] S. Ciarella, O. Gang, and F. Sciortino, "Toward the observation of a liquid-liquid phase transition in patchy origami tetrahedra: A numerical study," Eur. Phys. J. E **39**, 131 (2016).

[10] H. Tanaka, "Liquid–liquid transition and polyamorphism," J. Chem. Phys. **153**, 130901 (2020).

[11] H. E. Stanley and J. Teixeira, "Interpretation of the unusual behavior of H_2O and D_2O at low temperatures: Tests of a percolation model," J. Chem. Phys. **73**, 3404–3422 (1980).

[12] P. G. Debenedetti, "Supercooled and glassy water," J. Phys.: Condens. Matter **15**, R1669–R1726 (2003).

[13] R. J. Speedy and C. A. Angell, "Isothermal compressibility of supercooled water and evidence for a thermodynamic singularity at −45°C," J. Chem. Phys. **65**, 851–858 (1976).

[14] O. Mishima, "Reversible first order transition between two H_2O amorphs at 0.2 GPa and 135 K," J. Chem. Phys. **100**, 5910–5912 (1994).

[15] K. Amann-Winkel, C. Gainaru, P. H. Handle, M. Seidl, H. Nelson, R. Böhmer, and T. Loerting, "Water's second glass transition," Proc. Natl. Acad. Sci. U. S. A. **110**, 17720–17725 (2013).

[16] P. H. Handle, T. Loerting, and F. Sciortino, "Supercooled and glassy water: Metastable liquid(s), amorphous solid(s), and a no-man's land," Proc. Natl. Acad. Sci. U. S. A. **114**, 13336–13344 (2017).

[17] K. H. Kim, K. Amann-Winkel, N. Giovambattista, A. Späh, F. Perakis, H. Pathak, M. L. Parada, C. Yang, D. Mariedahl, T. Eklund, T. J. Lane, S. You, S. Jeong, M. Weston, J. H. Lee, I. Eom, M. Kim, J. Park, S. H. Chun, P. H. Poole, and A. Nilsson, "Experimental observation of the liquid-liquid transition in bulk supercooled water under pressure," Science **370**, 978–982 (2020).

[18] P. G. Debenedetti, F. Sciortino, and G. H. Zerze, "Second critical point in two realistic models of water," Science **369**, 289–292 (2020).

[19] J. L. F. Abascal, E. Sanz, R. García Fernández, and C. Vega, "A potential model for the study of ices and amorphous water: TIP4P/Ice," J. Chem. Phys. **122**, 234511 (2005).

[20] J. L. F. Abascal and C. Vega, "A general purpose model for the condensed phases of water: TIP4P/2005," J. Chem. Phys. **123**, 234505 (2005).

[21] T. E. Gartner, L. Zhang, P. M. Piaggi, R. Car, A. Z. Panagiotopoulos, and P. G. Debenedetti, "Signatures of a liquid–liquid transition in an ab initio deep neural network model for water," Proc. Natl. Acad. Sci. U. S. A. **117**, 26040–26046 (2020).

[22] E. R. Pinnick, S. Erramilli, and F. Wang, "Predicting the melting temperature of ice-Ih with only electronic structure information as input," J. Chem. Phys. **137**, 014510 (2012).

[23] A. J. Rusnak, E. R. Pinnick, C. E. Calderon, and F. Wang, "Static dielectric constants and molecular dipole distributions of liquid water and ice-Ih investigated by the PAW-PBE exchange-correlation functional," J. Chem. Phys. **137**, 034510 (2012).

[24] Y. Li, J. Li, and F. Wang, "Liquid–liquid transition in supercooled water suggested by microsecond simulations," Proc. Natl. Acad. Sci. U. S. A. **110**, 12209–12212 (2013).

[25] Y. Yuan, J. Li, X.-Z. Li, and F. Wang, "The strengths and limitations of effective centroid force models explored by studying isotopic effects in liquid water," J. Chem. Phys. **148**, 184102 (2018).

[26] V. Holten, J. C. Palmer, P. H. Poole, P. G. Debenedetti, and M. A. Anisimov, "Two-state thermodynamics of the ST2 model for supercooled water," J. Chem. Phys. **140**, 104502 (2014).

[27] R. S. Singh, J. W. Biddle, P. G. Debenedetti, and M. A. Anisimov, "Two-state thermodynamics and the possibility of a liquid-liquid phase transition in supercooled TIP4P/2005 water," J. Chem. Phys. **144**, 144504 (2016).

[28] R. Shi and H. Tanaka, "The anomalies and criticality of liquid water," Proc. Natl. Acad. Sci. U. S. A. **117**, 26591–26599 (2020).

[29] M. Invernizzi and M. Parrinello, "Rethinking metadynamics: From bias potentials to probability distributions," J. Phys. Chem. Lett. **11**, 2731–2736 (2019).

[30] P. M. Piaggi and M. Parrinello, "Multithermal-multibaric molecular simulations from a variational principle," Phys. Rev. Lett. **122**, 050601 (2019).

[31] O. Valsson and M. Parrinello, "A variational approach to enhanced sampling and free energy calculations," Phys. Rev. Lett. **113**, 090601 (2014).

[32] G. A. Tribello, M. Bonomi, D. Branduardi, C. Camilloni, and G. Bussi, "PLUMED 2: New feathers for an old bird," Comput. Phys. Commun. **185**, 604–613 (2013).

[33] G. Bussi, "Hamiltonian replica exchange in GROMACS: A flexible implementation," Mol. Phys. **112**, 379–384 (2014).

[34] H. E. Stanley and V. K. Wong, "Introduction to phase transitions and critical phenomena," Am. J. Phys. **40**, 927–928 (1972).

[35] N. B. Wilding and A. D. Bruce, "Density fluctuations and field mixing in the critical fluid," J. Phys.: Condens. Matter **4**, 3087–3108 (1992).

[36] M. M. Tsypin and H. W. Blöte, "Probability distribution of the order parameter for the 3D Ising model universality class: A high precision Monte Carlo study," Phys. Rev. E **62**, 73–76 (1999).

[37] A. M. Ferrenberg and R. H. Swendsen, "Optimized Monte Carlo data analysis," Phys. Rev. Lett. **63**, 1195–1198 (1989).

[38] A. Z. Panagiotopoulos, V. Wong, and M. A. Floriano, "Phase equilibria of lattice polymers from histogram reweighting Monte Carlo simulations," Macromolecules **31**, 912–918 (1998).

[39] J. W. Biddle, V. Holten, and M. A. Anisimov, "Behavior of supercooled aqueous solutions stemming from hidden liquid–liquid transition in water," J. Chem. Phys. **141**, 074504 (2014).

[40] K. Binder, "Critical properties from Monte Carlo coarse graining and renormalization," Phys. Rev. Lett. **47**, 693–696 (1981).

[41] M. J. Abraham, T. Murtola, R. Schulz, S. Páll, J. C. Smith, B. Hess, and E. Lindahl, "GROMACS: High performance molecular simulations through multi-level parallelism from laptops to supercomputers," SoftwareX **1-2**, 19–25 (2015).

[42] S. Pronk, S. Páll, R. Schulz, P. Larsson, P. Bjelkmar, R. Apostolov, M. R. Shirts, J. C. Smith, P. M. Kasson, D. van der Spoel, B. Hess, and E. Lindahl, "GROMACS 4.5: A high-throughput and highly parallel open source molecular simulation toolkit," Bioinformatics **29**, 845–854 (2013).

[43] B. Hess, C. Kutzner, D. van der Spoel, and E. Lindahl, "GROMACS 4: Algorithms for highly efficient, load-balanced, and scalable molecular simulation," J. Chem. Theory Comput. **4**, 435–447 (2008).

[44] D. van der Spoel, E. Lindahl, B. Hess, G. Groenhof, A. E. Mark, and H. J. Berendsen, GROMACS: Fast, flexible, and free, 2005.

[45] E. Lindahl, B. Hess, and D. van der Spoel, "GROMACS 3.0: A package for molecular simulation and trajectory analysis," J. Mol. Model. **7**, 306–317 (2001).

[46] H. J. C. Berendsen, D. van der Spoel, and R. van Drunen, "GROMACS: A message-passing parallel molecular dynamics implementation," Comput. Phys. Commun. **91**, 43–56 (1995).

[47] S. Nosé, "A molecular dynamics method for simulations in the canonical ensemble," Mol. Phys. **52**, 255–268 (1984).

[48] W. G. Hoover, "Canonical dynamics: Equilibrium phase-space distributions," Phys. Rev. A **31**, 1695–1697 (1985).

[49] M. Parrinello and A. Rahman, "Polymorphic transitions in single crystals: A new molecular dynamics method," J. Appl. Phys. **52**, 7182–7190 (1981).

[50] V. Holten and M. A. Anisimov, "Entropy-driven liquid–liquid separation in supercooled water," Sci. Rep. **2**, 713 (2012).

[51] L. Xu, P. Kumar, S. V. Buldyrev, S.-H. Chen, P. H. Poole, F. Sciortino, and H. E. Stanley, "Relation between the Widom line and the dynamic crossover in systems with a liquid–liquid phase transition," Proc. Natl. Acad. Sci. U. S. A. **102**, 16558–16562 (2005).

[52] L. Landau and I. M. Khalatnikov, "On the anomalous absorption of sound near a second order phase transition point (English translation in 'Collected Papers of Landau', edited by D. Ter Haar, 1965)," Dokl. Akad. Nauk SSSR **96**, 469 (1954).

[53] V. Bianco and G. Franzese, "Critical behavior of a water monolayer under hydrophobic confinement," Sci. Rep. **4**, 4440 (2015).

[54] R. Foffi, J. Russo, and F. Sciortino, "Structural and topological changes across the liquid–liquid transition in water," J. Chem. Phys. **154**, 184506 (2021).

[55] A. Nilsson and L. G. M. Pettersson, "The structural origin of anomalous properties of liquid water," Nat. Commun. **6**, 8998 (2015).

[56] V. Holten, C. E. Bertrand, M. A. Anisimov, and J. V. Sengers, "Thermodynamics of supercooled water," J. Chem. Phys. **136**, 094507 (2011).

[57] Y. Ni and J. L. Skinner, "Evidence for a liquid-liquid critical point in supercooled water within the E3B3 model and a possible interpretation of the kink in the homogeneous nucleation line," J. Chem. Phys. **144**, 214501 (2016).

[58] N. J. Hestand and J. L. Skinner, "Perspective: Crossing the Widom line in no man's land: Experiments, simulations, and the location of the liquid-liquid critical point in supercooled water," J. Chem. Phys. **149**, 140901 (2018).

[59] Y. Liu, A. Z. Panagiotopoulos, and P. G. Debenedetti, "Low-temperature fluid-phase behavior of ST2 water," J. Chem. Phys. **131**, 104508 (2009).

[60] K. H. Kim, A. Späh, H. Pathak, F. Perakis, D. Mariedahl, K. Amann-Winkel, J. A. Sellberg, J. H. Lee, S. Kim, J. Park, K. H. Nam, T. Katayama, and A. Nilsson, "Maxima in the thermodynamic response and correlation functions of deeply supercooled water," Science **358**, 1589–1593 (2017).

[61] A. Späh, H. Pathak, K. H. Kim, F. Perakis, D. Mariedahl, K. Amann-Winkel, J. A. Sellberg, J. H. Lee, S. Kim, J. Park, K. H. Nam, T. Katayama, and A. Nilsson, "Apparent power-law behavior of water's isothermal compressibility and correlation length upon supercooling," Phys. Chem. Chem. Phys. **21**, 26–31 (2019).

[62] H. Pathak, A. Späh, K. H. Kim, I. Tsironi, D. Mariedahl, M. Blanco, S. Huotari, V. Honkimäki, and A. Nilsson, "Intermediate range O–O correlations in supercooled water down to 235 K," J. Chem. Phys. **150**, 224506 (2019).

[63] F. Gao and L. Han, "Implementing the Nelder-Mead simplex algorithm with adaptive parameters," Comput. Optim. Appl. **51**, 259–277 (2012).

[64] P. J. Steinhardt, D. R. Nelson, and M. Ronchetti, "Bond-orientational order in liquids and glasses," Phys. Rev. B **28**, 784–805 (1983).

[65] F. James and M. Roos, "Minuit—A system for function minimization and analysis of the parameter errors and correlations," Comput. Phys. Commun. **10**, 343–367 (1975).